DOI: 10.23968/2500-0055-2023-8-4-82-98

FREE VIBRATION MODELING IN A FUNCTIONALLY GRADED HOLLOW CYLINDER USING THE LEGENDRE POLYNOMIAL APPROACH

Rabab Raghib[1]*, Ismail Naciri[1], Hassna Khalfi[1], Lahoucine Elmaimouni[1], Jiangong Yu[2], Abdelmajid Bybi[3], Mustapha Sahal[1]

[1]Ibn Zohr University, Polydisciplinary Faculty of Ouarzazate, BP.638, 45000 Ouarzazate, Morocco
[2]School of Mechanical and Power Engineering, Henan Polytechnic University, Jiaozuo 454003, China
[3]Mohammed V University in Rabat, Higher School of Technology in Salé, Materials, Energy and Acoustics Team (MEAT), Morocco

*Corresponding author's e-mail: rababraghib97@gmail.com

Abstract

Introduction: The building industry is under increasing pressure to maximize performance while reducing the costs and the environmental impact. To solve this problem, a new type of materials, i.e., functionally graded materials (FGMs), are proposed. These materials have the advantage of being able to withstand harsh environments without losing their properties. **Purpose of the study:** The paper aims to further extend the understanding of the propagation modes and characteristics of guided waves in FGM cylinders with infinite lengths. In the course of the study, we analyzed a cylindrical shell composed of three annular layers, each separated by a gradient layer across the wall thickness. A modeling tool based on the Legendre orthogonal polynomial method is proposed in the paper. **Methods:** The method applied results in an eigenvalue/eigenvector problem. The boundary conditions are integrated into the constitutive equations of guided wave propagation. The phase velocity and normalized frequency dispersion curves are calculated. Besides, the displacement distributions and stress field profiles for a functionally graded cylinder with various graded indices in both modes (axisymmetric and symmetric) are calculated and discussed. The results show a constant fluctuation of effective FGM material. **Results:** It was found that the phase velocity curves of the same mode decrease as the exponents of the power law increase. In addition, the boundary conditions have a greater impact on the normal stresses. The accuracy and effectiveness of the improved orthogonal polynomial method are demonstrated through a comparison of the exact solution obtained by an analytical-numerical method and our numerical results.

Keywords: guided waves, Legendre polynomial method, functionally graded materials (FGMs), dispersion curves.

Introduction

Material structures are becoming more complex and delicate due to recent scientific advancements in materials. Functionally graded materials (FGMs) have emerged as a result of exciting developments in engineering and material processing. FGMs are created in order to achieve higher levels of performance. In fact, FGMs are a class of composite materials with graded structure and characteristics changing spatially in the thickness direction. These materials have a graded interface rather than a sharp interface between two dissimilar materials. The purpose of choosing graded materials, particularly at the interface between layers, is to reduce inter-laminar stress discontinuities. These can occur around the edges of laminates due to material incompatibility across the interface. The interface between two layers in FGM is typically seen as having seamless bonding, with properties that progressively change based on their thickness. The properties of FGM change continuously from one surface to another due to the effective monotonic variation in the volume fraction of the constituent phases. That enables the elimination of stress discontinuity in most searches, including layered structures made of two materials. The primary advantage of these materials is their ability to adjust specific thermomechanical properties through a continuous spatial distribution, resulting in increased resistance to interfacial failure (Yang and Liu, 2020). Another advantage is their ability to withstand various external factors such as temperature or thickness gradients while maintaining their structural integrity (Gong et al., 1999).

Due to their graded properties in several dimensions, many researchers have focused greater attention on FGMs, utilizing a variety of techniques and mathematical approaches. Among those, the finite element method has become the most widely used for their structural analysis. Wang and Pan (2011) used the three-dimensional finite element method to investigate the behavior of FGM multiferroic composites under different types of loads. Hedayatrasa et al. (2014) used the time-domain spectral finite element method based on Chebyshev Lagrangian expansion to numerically describe the characteristics of elastic wave propagation in 2D FGMs. Using an analytical method, Gong et al. (1999) investigated the effects of the constituent volume

For citations: Raghib, R., Naciri, I., Khalfi, H., Elmaimouni, L., Yu, J., Bybi, A., Sahal, M. (2023). Free vibration modeling in a functionally graded hollow cylinder using the Legendre polynomial approach. Architecture and Engineering, No 4 (8), pp. 82-98. DOI: 10.23968/2500-0055-2023-8-4-82-98.

fraction on various structures of FG shells. Other researchers applied the same method to investigate elastic waves in an FG cylinder (Han et al., 2002) and an FG piezoelectric cylinder (Han and Liu, 2003). Furthermore, higher-level modeling techniques such as the Legendre polynomial series approach were developed to improve its accuracy. Some researchers also studied guided wave dispersion curves and displacement distributions in FGM plates (Lefebvre et al., 2001) and radially graded cylinders (Elmaimouni et al., 2005). This approach was further developed to explain the behavior of guided waves in more complex structures, including thermoelastic (Yu et al., 2010) and viscoelastic FGM plates (Yu et al., 2012) as well as functionally graded piezoelectric-piezomagnetic plates (Zhang et al., 2018). Liu et al. (2021) relied on the modified couple stress theory to examine the Lamb wave propagation properties in a small-scale functionally graded piezoelectric plate. Several other methods were utilized to analytically solve the wave equations in FGMs (Ashida et al., 2022; Bezzie & Woldemichael, 2021; Bian et al., 2022; Radman et al., 2023; Velhinho & Rocha, 2011; Wang et al., 2022).

The study of elastic wave propagation and dispersion is essential in the most diverse applications and domains like earthquake engineering, architecture and non-destructive testing (Yilmaz et al., 2020). The use of ultrasonic guided waves represents a rapid, effective, and delicate non-destructive testing method commonly employed for various engineering materials. Zhang et al. (2022b) explored the influence of polarization variation on phonon modes and phason modes in the quasi-periodic direction. Based on the Legendre polynomial method, Li et al. (2022) studied the propagation of longitudinal axisymmetric guided waves in a full-length bonding resin bolt, which is a bilayer structure. Zhang et al. (2022a) analyzed the propagation of generalized thermo-elastic waves in bars with a rectangular cross-section. Naciri et al. (2019) investigated the numerical vibrational characterization of an annular piezoelectric disc resonator partially covered with electrodes to express the mechanical displacement components as well as the electric potential.

In this perspective, the current research intends to provide an analytical framework to investigate wave propagation properties in a composite functionally graded (FG) structure made of stainless steel (SS) and silicon nitride (SN). In particular, it aims to numerically analyze wave propagation in a three-layered (SS/SN/SS) FGM cylinder. For this purpose, the volume fraction distribution is used to confirm that Young's modulus, Poisson's ratio, and the density of FGM cylinders vary gradually in the radial direction. Mathematical equations are converted into a complex eigenvalue and eigenvector problem, enabling the calculation of dispersion curves for normalized frequencies and phase velocity. The numerical results enable the evaluation of dispersion curves for longitudinal, torsional, and flexural modes. We also studied displacement distributions and stress field profiles to reveal and extend our understanding of the characteristics of guided waves in FG materials. The results of our comprehensive model are in line with the theoretical numerical results found in literature.

Methods

In this paper, the Legendre orthogonal polynomial method is proposed to model guided wave propagation in a multi-layered functionally graded hollow cylinder. In fact, the propagation of guided waves and their physical properties still remain an essential tool in several application domains, such as: non-destructive testing and evaluation (NDT&E) (Yilmaz et al., 2020) and structural health monitoring (SHM) (Wang et al., 2020). In this case, the acoustic waves are reflected when they encounter changes in the characteristic properties or geometry of materials, caused by specific phenomena, e.g., corrosion, discontinuities, welds, etc., thus making it possible to localize defects and providing information about their nature. This simplifies testing over long distances and prevents the need to scan the entire structure. Thanks to this method, it is possible to inspect even hard-to-reach areas without having to remove the insulation material in certain cases (Huang et al., 2020). This study represents a crucial step for non-destructive evaluation (NDE) of material properties and, therefore, for better understanding of its potential applications in manufacturing and quality control. The scope of this research could be expanded to encompass numerous other applications, including aeronautics, biomechanics, biomedicine, and automotive. Besides, FGMs are suitable for aerospace applications due to their ability to withstand extremely high thermal gradients. FGMs were first created for the aerospace sector. Their use has since expanded to cover components of rocket engines, heat exchangers, turbine wheels, turbine blades, space shuttles, and other machines (Ghatage et al., 2020).

Basic equation

In this section, a hollow FGM cylinder with infinite length is used to describe the problem as a part of the three-dimensional linear elasticity theory with various material parameters (Poisson's ratio v, density ρ, and Young's modulus E) varying in the radial direction, where *a* and *b* are the inner and outer radius, respectively. Let us also introduce such values as *H*, which is the thickness, and *R*, which is the average surface radius of the cylinder, with $H = b - a$ and $R = (a + b)/2$ as shown in Fig. 1.

The problem will be solved in a cylindrical coordinate system (*r*, φ, *z*), where *r*, φ, and *z* are

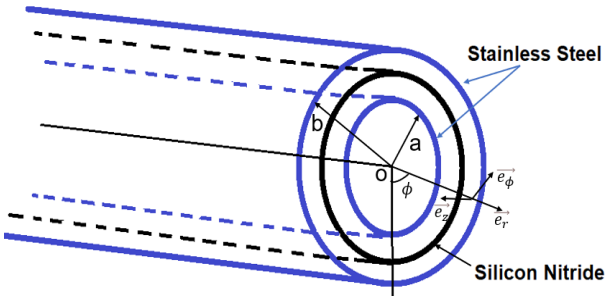

Fig. 1. FGM cylindrical structure with the (SS/SN/SS) configuration

the radial, circumferential, and axial directions, respectively. As the first assumption, the propagation of the acoustic waves is considered throughout the z-axis.

The usual approach is to start from an infinitesimal element in an infinite elastic isotropic solid with density ρ. In this case, a change of variable is proposed to solve the wave equations for circular cylinders:

$$q_1 = k\,r,\ q_2 = \varphi,\ q_3 = k\,z,$$

where *k* is the wave number.

The following equations can be used to represent the law of variation of stiffness $C_{ij}^{(M)}$ and density $\rho^{(M)}$ as a polynomial with degree L:

$$C_{ij}^{(M)}(q_1) = C_{ij}^{(0)} + C_{ij}^{(1)}\left(\frac{q_1}{kH}\right)^1 + C_{ij}^{2}\left(\frac{q_1}{kH}\right)^2 + \\ + \ldots\ldots\ldots + C_{ij}^{L}\left(\frac{q_1}{kH}\right)^L; \qquad (1.a)$$

$$\rho^{(M)}(q_1) = \rho^{(0)} + \rho^{(1)}\left(\frac{q_1}{kH}\right)^1 + \rho^{(2)}\left(\frac{q_1}{kH}\right)^2 + \\ + \ldots\ldots\ldots + \rho^{(L)}\left(\frac{q_1}{kH}\right)^L, \qquad (1.b)$$

where:

$C_{ij}^{(M)}(q_1)$, $i, j = 1, 2, \ldots 6$ are the ordinary elastic constants of the space constituting the cylinder at the point $M(q_1)$.

$\rho^{(M)}(q_1)$ is the density of the structure at the point $M(q_1)$.

In FGM hollow cylinders, the radial variation of material properties is considered progressive (Elmaimouni, 2005). As a result, material characteristics may be described in terms of q_1. Using the Einstein summation convention, Eq. 1.b can be expressed as follows:

$$\begin{cases} C_{ij}^{(M)}(q_1) = C_{ij}^{(l)}\left(\frac{q_1}{kH}\right)^l \\ \rho^{(M)}(q_1) = \rho^{(l)}\left(\frac{q_1}{kH}\right)^l \end{cases} \quad l = 0, 1, 2, \ldots\ldots L, \qquad (2)$$

where:

$C_{ij}^{(l)}$ and $\rho^{(l)}$ are the coefficients of a polynomial with degree l.

In a cylindrical coordinate system, the relationship between the deformation tensors and the displacement components for an elastic medium was described by Zhang et al. (2022a):

$$\begin{cases} \varepsilon_{rr} = \frac{\partial u_1}{\partial q_1} \\ \varepsilon_{\varphi\varphi} = \frac{u_1}{q_1} + \frac{1}{q_1}\frac{\partial u_2}{\partial q_2}, \\ \varepsilon_{zz} = \frac{\partial u_3}{\partial q_3} \end{cases} \quad \begin{cases} \varepsilon_{\varphi z} = \frac{1}{2}\left(\frac{\partial u_2}{\partial q_3} + \frac{1}{q_1}\frac{\partial u_3}{\partial q_2}\right) \\ \varepsilon_{rz} = \frac{1}{2}\left(\frac{\partial u_1}{\partial q_3} + \frac{\partial u_3}{\partial q_1}\right) \\ \varepsilon_{r\varphi} = \frac{1}{2}\left(\frac{1}{q_1}\frac{\partial u_1}{\partial q_2} + \frac{\partial u_2}{\partial q_1} - \frac{u_2}{q_1}\right) \end{cases}, \qquad (3)$$

where u_1, u_2 and u_3 are the components of mechanical displacement in the radial, circumferential, and axial directions, respectively.

According to the three-dimensional theory of elasticity, Hooke's law describes the properties of both homogeneous and inhomogeneous materials. For each layer, the stress-strain expressions can be represented as follows (Elmaimouni, 2005):

$$\begin{cases} T_{rr} = C_{11}^{l}\left(\frac{q_1}{kH}\right)^l \frac{\partial u_1}{\partial r} + C_{12}^{l}\left(\frac{q_1}{kH}\right)^l \left(\frac{u_1}{r} + \frac{1}{r}\frac{\partial u_2}{\partial \varphi}\right) + \\ \qquad + C_{13}^{l}\left(\frac{q_1}{kH}\right)^l \frac{\partial u_3}{\partial z} \\ T_{\varphi\varphi} = C_{12}^{l}\left(\frac{q_1}{kH}\right)^l \frac{\partial u_1}{\partial r} + C_{22}^{l}\left(\frac{q_1}{kH}\right)^l \left(\frac{u_1}{r} + \frac{1}{r}\frac{\partial u_2}{\partial \varphi}\right) + \\ \qquad + C_{23}^{l}\left(\frac{q_1}{kH}\right)^l \frac{\partial u_3}{\partial z} \\ T_{zz} = C_{13}^{l}\left(\frac{q_1}{kH}\right)^l \frac{\partial u_1}{\partial r} + C_{23}^{l}\left(\frac{q_1}{kH}\right)^l \left(\frac{u_1}{r} + \frac{1}{r}\frac{\partial u_2}{\partial \varphi}\right) + \\ \qquad + C_{33}^{l}\left(\frac{q_1}{kH}\right)^l \frac{\partial u_3}{\partial z} \\ T_{\varphi z} = C_{44}^{l}\left(\frac{q_1}{kH}\right)^l \left(\frac{\partial u_2}{\partial z} + \frac{1}{r}\frac{\partial u_3}{\partial \varphi}\right) \\ T_{rz} = C_{55}^{l}\left(\frac{q_1}{kH}\right)^l \left(\frac{\partial u_1}{\partial z} + \frac{1}{r}\frac{\partial u_3}{\partial r}\right) \\ T_{r\varphi} = C_{66}^{l}\left(\frac{q_1}{kH}\right)^l \left(\frac{1}{r}\frac{\partial u_1}{\partial \varphi} + \frac{\partial u_2}{\partial r} - \frac{u_2}{r}\right) \end{cases}, \qquad (4)$$

where T_{ij} denote the components of the stress tensor and C_{ijkl} denote the elastic coefficients.

By neglecting the body force, we can write the three-dimensional stress motion equations and displacement components of a linear elastic material in cylindrical coordinates as follows (Li et al., 2022):

$$\frac{\partial T_{rr}}{\partial r} + \frac{1}{r}\frac{\partial T_{r\varphi}}{\partial \varphi} + \frac{\partial T_{rz}}{\partial z} + \frac{T_{rr} - T_{\varphi\varphi}}{r} = \rho\frac{\partial^2 u_1}{\partial t^2};$$

$$\frac{\partial T_{r\varphi}}{\partial r}+\frac{1}{r}\frac{\partial T_{\varphi\varphi}}{\partial \varphi}+\frac{\partial T_{\varphi z}}{\partial z}+\frac{2T_{r\varphi}}{r}=\rho\frac{\partial^2 u_2}{\partial t^2};\qquad(5)$$

$$\frac{\partial T_{rz}}{\partial r}+\frac{1}{q_1}\frac{\partial T_{\varphi z}}{\partial \varphi}+\frac{\partial T_{zz}}{\partial z}+\frac{T_{rz}}{r}=\rho\frac{\partial^2 u_3}{\partial t^2}.$$

Boundary conditions

The electrical and mechanical boundary conditions are embedded directly into the equations of motion, using position-dependent physical quantities $C_{ij}(q_1)$ and rectangular window functions $\pi(ka,kb)$ (Elmaimouni et al., 2005; Lefebvre et al., 2001; Naciri et al., 2019), defined according to the studied geometrical structure, in order to take into consideration the entire surface of the studied structure without the need of meshing. Thus, the cylindrical structure can be defined as follows:

$$ka\le q_1\le kb,\ 0\le q_2\le 2\pi,\ -\infty\le q_3\le+\infty$$

When the boundary condition of the material is taken into account, the position-dependent elastic constants and density can be obtained by the following expressions:

$$\begin{cases} C_{ij}^{(M)}(q_1)=C_{ij}^{(l)}\left(\dfrac{q_1}{kH}\right)^l\pi(ka,kb)\\ \rho_{ij}^{(M)}(q_1)=\rho_{ij}^{(l)}\left(\dfrac{q_1}{kH}\right)^l\pi(ka,kb)\end{cases},\qquad(6)$$

where:

$\pi(ka,kb)$ is the rectangular window function defined as follows:

$$\pi(ka,kb)=\begin{cases}1 & ka\le q_1\le kb\\ 0 & \text{elsewhere}\end{cases}.\qquad(7)$$

According to Eqs. 6 and 7, the density and the elastic modulus in the outer cylinder are equal to zero. As a result, the vacuum outside the cylinder is regarded as a medium with zero impedance, which ensures that the stresses outside the cylinder are equal to zero.

Mechanical displacements

Since in this research guided waves are assumed to propagate in the z-direction, the components of the mechanical displacement in an orthonormal basis can be represented as follows:

$$u_1(q_1,q_2,q_3,t)=\frac{1}{\sqrt{2\pi}}e^{inq_2}e^{i(\omega t-q_3)}\sum_{m=0}^{\infty}p_m^1Q_m(q_1);\qquad(8.a)$$

$$u_2(q_1,q_2,q_3,t)=\frac{1}{\sqrt{2\pi}}e^{inq_2}e^{i(\omega t-q_3)}\sum_{m=0}^{\infty}p_m^2Q_m(q_1);\qquad(8.b)$$

$$u_3(q_1,q_2,q_3,t)=\frac{1}{\sqrt{2\pi}}e^{inq_2}e^{i(\omega t-q_3)}\sum_{m=0}^{\infty}p_m^3Q_m(q_1).\qquad(8.c)$$

where n = 0, 1, 2, ... — the circumferential wave number, ω — the pulsation, $p_m^{\alpha}(\alpha=1,2\ et\ 3)$ — the amplitudes of the polynomial Q_m, $\alpha=1$ pertains to the radial direction, $\alpha=2$ pertains to the circumferential direction, and $\alpha=3$ pertains to the axial direction. The polynomials $Q_m(q_1)$ can be written as follows:

$$Q_m(q_1)=\sqrt{\frac{2m+1}{kH}}P_m\left(\frac{2q_1-(kR_2+kR_1)}{kH}\right),$$

where:

P_m is the Legendre polynomial with degree *m*,

$Q_m(q_1)$ is the complete orthonormal set in the range $ka\le q_1\le kb$, which can represent any continuous function. Each of these three components of mechanical displacements is represented by a set of three functions. The functions associated with the circumferential and axial terms are expressed by exponential functions while the radial term is represented by Legendre polynomials (Yilmaz et al., 2020).

The stress tensors in Eq. 4 and the mechanical displacement in Eq. 8 can be embedded into the motion equations given in Eq. 5, and the derivatives of the rectangular window function $\pi(ka,kb)$ produce terms $\delta(q_1=ka)$ and $\delta(q_1=kb)$. Such formulation gives us the equation system shown below:

$$\begin{bmatrix} C_{11}^{(l)}q_1^{\,l+2}\dfrac{\partial^2 u_1}{\partial q_1^2}+(1+l)C_{11}^{(l)}q_1^{\,l+1}\dfrac{\partial u_1}{\partial q_1}+\\ +(lC_{12}^{(l)}-C_{22}^{(l)}-n^2C_{66}^{(l)})q_1^{\,l}u_1-\\ -C_{55}^{(l)}q_1^{\,l+2}u_1-in(C_{12}^{(l)}+C_{66}^{(l)})q_1^{\,l+1}\dfrac{\partial u_2}{\partial q_1}+\\ +in(lC_{22}^{(l)}-C_{66}^{(l)}-C_{12}^{(l)})q_1^{\,l}u_2-i(C_{13}^{(l)}+\\ +C_{55}^{(l)})q_1^{\,l+2}\dfrac{\partial u_3}{\partial q_1}-i((1+l)C_{13}^{(l)}-C_{23}^{(l)})q_1^{\,l+1}u_3 \end{bmatrix}\times$$

$$\times\frac{1}{(kH)^l}\pi(ka,kb)+$$

$$+\frac{1}{(kH)^l}\begin{bmatrix} C_{11}^{(l)}q_1^{\,l+2}\dfrac{\partial u_1}{\partial q_1}+C_{12}^{(l)}q_1^{\,l+1}u_1+\\ +inC_{12}^{(l)}q_1^{\,l+1}u_2-iC_{13}^{(l)}q_1^{\,l+2}u_3 \end{bmatrix}\times$$

$$\times\left(\delta(q_1=ka)-\delta(q_1=kb)\right)=$$

$$=-\rho^{(l)}\left(\frac{\omega}{k}\right)^2\frac{1}{(kH)^l}q_1^{l+2}u_1\pi(ka,kb);\qquad(9.a)$$

$$\begin{bmatrix} in(C_{12}^{(l)}+C_{66}^{(l)})q_1^{\,l+1}\dfrac{\partial u_1}{\partial q_1}+in(C_{22}^{(l)}+\\ +(1+l)C_{66}^{(l)})q_1^{\,l}u_1-(n^2C_{22}^{(l)}+\\ +(1+l)C_{66}^{(l)})q_1^{\,l}u_2+C_{66}^{(l)}q_1^{\,l+2}\dfrac{\partial^2 u_2}{\partial q_1^2}+\\ +(1+l)C_{66}^{(l)}q_1^{\,l+1}\dfrac{\partial u_2}{\partial q_1}-C_{44}^{(l)}q_1^{\,l+2}u_2+\\ +n(C_{23}^{(l)}+C_{44}^{(l)})q_1^{\,l+1}u_3 \end{bmatrix}\times$$

$$\times\frac{1}{(kH)^l}\pi(ka,kb)+$$

$$+\frac{1}{(kH)^l}\left[C_{66}^{(l)}\left(inq_1{}^{l+1}u_1+q_1{}^l\frac{\partial u_2}{\partial q_1}-q_1{}^{l+1}u_2\right)\right]\times \quad (9.b)$$

$$\times\left(\delta(q_1=ka)-\delta(q_1=kb)\right)=$$

$$=-\rho^{(l)}\left(\frac{\omega}{k}\right)^2\frac{1}{(kH)^l}q_1^{l+2}u_2\pi(ka,kb);$$

$$\left[\begin{array}{l}-i(C_{13}^{(l)}+C_{55}^{(l)})q_1^{l+2}\dfrac{\partial u_1}{\partial q_1}-\\ -i(C_{23}^{(l)}+(1+l)C_{55}^{(l)})q_1^{l+1}u_1+\\ +n(C_{23}^{(l)}+C_{44}^{(l)})q_1^{l+1}u_2+\\ +C_{55}^{(l)}q_1^{l+2}\dfrac{\partial^2 u_3}{\partial q_1^2}-n^2C_{44}^{(l)}q_1^l u_3-\\ -C_{33}^{(l)}q_1^{l+2}u_3+(1+l)C_{55}^{(l)}q_1^{l+1}\dfrac{\partial u_3}{\partial q_1}\end{array}\right]\times$$

$$\times\frac{1}{(kH)^l}\pi(ka,kb)+$$

$$+\left[-iC_{55}^{(l)}q_1^{l+2}u_1+C_{55}^{(l)}q_1^{l+2}\frac{\partial u_3}{\partial q_1}\right]\frac{\partial}{\partial q_1}\pi(ka,kb)=$$

$$=-\rho^{(l)}\left(\frac{\omega}{k}\right)^2\frac{1}{(kH)^l}q_1^{l+2}u_3\pi(ka,kb). \quad (9.c)$$

Each element of Eq. 9 (a–c) was multiplied by $\frac{1}{\sqrt{2\pi}}Q_j^*(q_1)e^{-inq_2}$, with *j* varying from 0 to infinity. The obtained equations were integrated over *j* from 0 to infinity, over q_1 from kR_1 to kR_2, and over q_2 from 0 to 2π. Thus, we can deduce the following system of equations:

$$\begin{aligned}&{}^lA_{11}^{m,j}p_m^1+{}^lA_{12}^{m,j}p_m^2+{}^lA_{13}^{m,j}p_m^3=-\eta^2\,{}^lM_j^m p_m^1;\\ &{}^lA_{21}^{m,j}p_m^1+{}^lA_{22}^{m,j}p_m^2+{}^lA_{23}^{m,j}p_m^3=-\eta^2\,{}^lM_j^m p_m^2; \quad (10)\\ &{}^lA_{31}^{m,j}p_m^1+{}^lA_{32}^{m,j}p_m^2+{}^lA_{33}^{m,j}p_m^3=-\eta^2\,{}^lM_j^m p_m^3.\end{aligned}$$

These characteristic equations may be expressed as the product of two matrices with the following eigenvalues and eigenvectors:

$$\left[\left({}^lM\right)^{-1}{}^lA\right]_{\alpha\beta}^{m,j}p_m^\alpha=-\eta^2\,p_m^\alpha \quad (11)$$

The guided velocity is as follows: $\eta^2=\rho V_{ph}^2$, $V_{ph}=\omega/k$.

$p_m^\alpha\ (\alpha=1,2\ and\ 3)$ is the eigenvector enabling the calculation of the displacement components and all other associated field parameters.

${}^lA_{\alpha\beta}^{m,j}\ (\alpha,\beta=1,2,3)$, ${}^lM_j^m$ are the equations required to calculate all the matrix elements (more details are given in the Appendix below).

All the equations required to calculate the pertinent matrix elements are provided in the Appendix below. A three-layered FGM cylinder is examined using the suggested approach following the above derivation steps. In this regard, MATLAB software is used to numerically solve the matrix of eigenvalues and eigenvectors in Eq. 11. Finally, we point out that when the wave number *k* and the graded index change, the eigenvalue problem is resolved using MATLAB eig function. Eigenvectors can be used to define the wave profile, and eigenvalues — to calculate the phase velocity. As a result, it is clear that the suggested approach represents an efficient way to simultaneously acquire the displacement, stress distribution and dispersion curves of an FGM cylinder.

Results and discussion

Configurations of cylindrical FGM structures

In order to verify the accuracy and effectiveness of our polynomial approach, we examined the acoustic waves in a three-layered hollow inhomogeneous cylinder made of two different materials, as discussed by Gong et al. (1999) and Han et al. (2002) and shown in Figure 1. In our investigation, silicon nitride and stainless steel were used. FG cylinders have silicon nitride (SN) at the central surface and stainless steel (SS) on the exterior and interior. Table lists the elastic properties of stainless steel and silicon nitride required to solve the FGM frequency equation.

A computer program was developed to calculate the dispersion behavior using the preceding equation. In this case, the Voigt-type model is applied to determine the effective FGM property of two mixed materials at the i^{th} layer level. It can be written as follows:

$$f^{(i)}(q_1)=f_1^{(i)}V_{m1}^{(i)}(q_1)+f_2^{(i)}V_{m2}^{(i)}(q_1);\ i=1,2.....k, \quad (12)$$

where $f^{(i)}$ is the effective material proportion of FGM and the volume fraction, $V_{mj}^{(i)}(q_1)$ is the j^{th} material volume fraction with $V_{m1}^{(i)}(q_1)+V_{m2}^{(i)}(q_1)=1$.

In case of FGM structures, the displacement and stress components should be continuous at the interfaces between the layers due to the advantages of the monotonic change in the volume fraction of the phase components, which allows the elimination of stress discontinuities. These considerations are adopted to align with those utilized by Gong et al. (1999) for validation, with position to thickness ratio $\frac{q_1}{kH}$ in the range from -1 to 1. Additionally, the shape of the local volume fraction is shown as a power series *S* using the following equation in the radial direction:

$$\begin{cases} V_{m1}^{(1)}(q_1) = \left[\left(\dfrac{q_1 - ka}{kH}\right)^2\right]^S \\ V_{m2}^{(1)}(q_1) = 1 - V_{m1}^{(1)}(q_1) \end{cases} \quad -\frac{ka}{kH} \le q_1 \le 0;$$

$$\begin{cases} V_{m1}^{(2)}(q_1) = \left[\left(\dfrac{q_1 + ka}{kH}\right)^2\right]^S \\ V_{m2}^{(2)}(q_1) = 1 - V_{m1}^{(1)}(q_1) \end{cases} \quad 0 \le q_1 \le \frac{kb}{kH}. \quad (13)$$

This research examines a three-layered FGM cylinder. Here, $V_{m1}^{(i)}$ is the volume fraction of silicon nitride, and $V_{m2}^{(i)}$ is the volume fraction of stainless steel in the (SS/SN/SS) cylinder arrangement. It is assumed that the values of the gradient index *S* vary from 0.1 to 25 for the functionally graded material along the radial direction. The variation tendency of volume fraction distribution along the radial direction significantly changed due to gradient exponents, as observed in Fig. 2. The amount of silicon nitride in the inner layer of the FGM cylinder equals 0, increasing continuously to 1 at the middle surface $\left(\frac{q_1}{kH} = 0\right)$ as the gradient index *S* rises before continually decreasing to 0 in the outer layer. As for the stainless steel volume fraction, it roughly decreases from 1 in the inner layer to 0 at the middle surface as the gradient exponent grows, and then exponentially increases to 1 at the outer surface. This proves that in the inner layer $\left(\frac{q_1}{kH} = -1\right)$ and the outer layer $\left(\frac{q_1}{kH} = 1\right)$, the surface is uniformly dominated by stainless steel, whereas at the middle surface $\left(\frac{q_1}{kH} = 0\right)$, the silicon nitride volume fraction is dominant.

Based on Eqs. 12 and 13, we have calculated the spatial distributions of the mechanical characteristics of the FGM cylinder along the thickness direction. Figs. 3(a-c) show the variations of FGM Young's modulus, Poisson's ratio, and density for the (SS/SN/SS) configuration with the variation of the power-law exponent (*S*) across the radial direction when *S* = 0.1, 0.3, 0.5, 1, 2, and 4. Furthermore, it is possible to calculate the stiffness coefficient $C_{ij}^{(l)}$ of order l of the examined FGM based on Poisson's ratio $\nu(q_1)$, density $\rho^{(l)}$, and Young's modulus $E(q_1)$ of the silicon nitride and stainless steel volume fractions previously determined using Eq. 12. As for the numerical results, the coefficients $C_{11}^{(l)}$, $C_{12}^{(l)}$ and $C_{44}^{(l)}$ of the studied FGM are shown in Fig. 4. It can be observed that Poisson's ratio, density, Young's modulus, and position-dependent elastic constants $C_{ij}^{(l)}$ of the functionally graded material vary continuously along the radial direction. This research also demonstrates a significant influence of the graded index on changes in material properties in the radial direction q_1 when $kH = ka$.

Dispersion curves

The resolution of the system of equations (10) results in the dispersion curves of the propagation modes in the structure, relating the frequencies (*f*) to the wave numbers (*k*). In this context, a computer program was developed to plot the dispersion curves of cylindrical structures. We decided to express the phase velocities as a function of frequency-thickness. Moreover, the

Stainless steel and silicon nitride material properties

	Properties		
	E (GPa)	ν	ρ (kg/m³)
Silicon nitride	322.4	0.24	2370
Stainless steel	207.82	0.317	8166

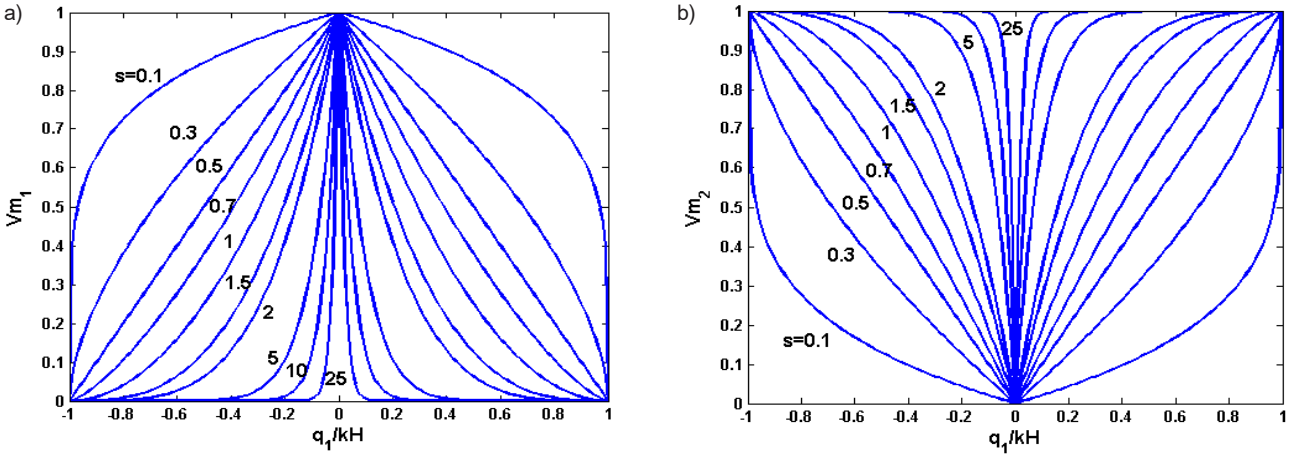

Fig. 2. Variation of the volume fraction in the cylindrical layer of FGM in the radial direction with different graded index *S* values: (a) volume fraction of silicon nitride (b) volume fraction of stainless steel

numerical results are used to demonstrate how the graded index affects the convergence of dispersion curves. It provides a theoretical support for the quantitative measurement of the structural properties of the FGM cylinder by utilizing the relationship between the gradient distribution and propagation characteristics. Figs. 5 and 6 show the dispersion curves for the (SS/SN/SS) configuration of the FGM cylinder for axisymmetric (longitudinal L(0, m), torsional T(0, m)) and symmetric (F(1, m)) modes, respectively. It can be noticed that for all propagation modes for the functionally graded cylinder in the (SS/SN/SS) configuration, only the first modes L(0,1), T(0,1) and F(0,1) did not show any cut-off frequencies.

In this section, the relationship between the guided wave phase velocity and gradient distribution is examined. Figs. 7 and 8 present the phase velocity curves of the axisymmetric (n = 0) and symmetric (n = 1) modes of the configuration (SS/SN/SS) as a function of the frequency (f)-thickness (H) product, where H/R = 1.

In this study, only three mode values are taken into account: 0.1, 1, and 4. Figs. 7 and 8 show that all modes are dispersive. Besides, it was found that only the first modes (the lowest modes) did not have any cut-

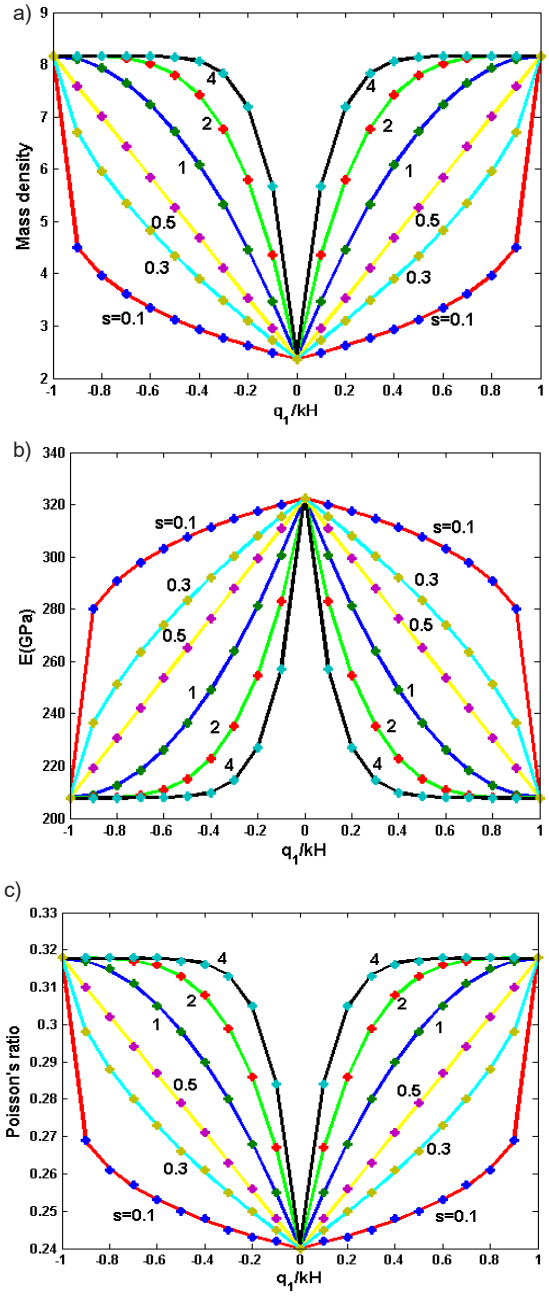

Fig. 3. Spectral variation of: (a) Poisson's ratio, (b) density, (c) Young's modulus

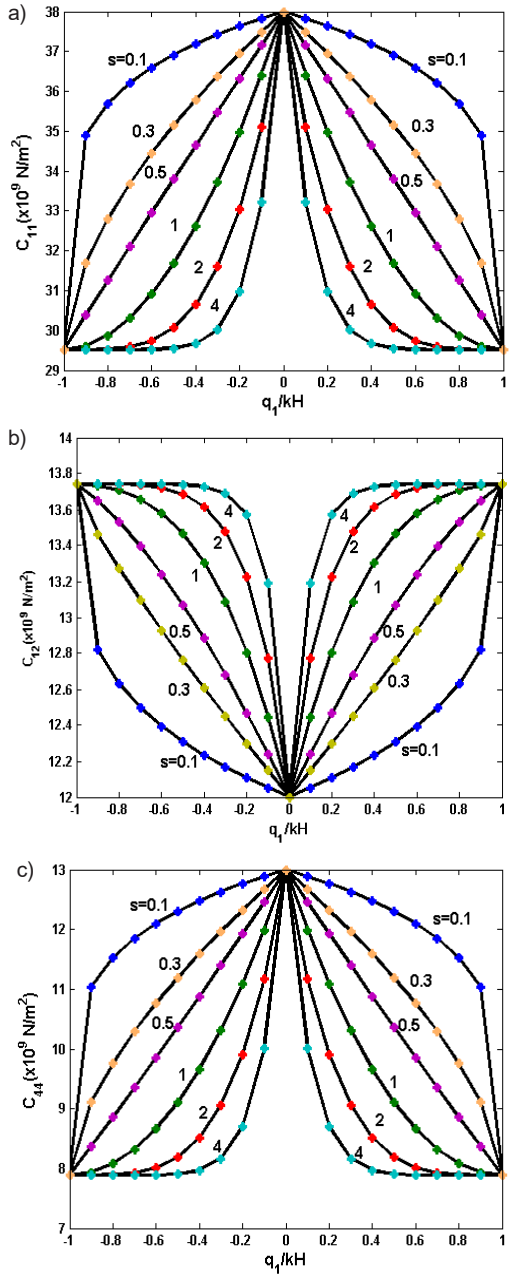

Fig. 4. Spectral variation of the stiffness coefficient $c_{ij}^{(l)}$: (a) $c_{11}^{(l)}$, (b) $c_{12}^{(l)}$, (c) $c_{44}^{(l)}$

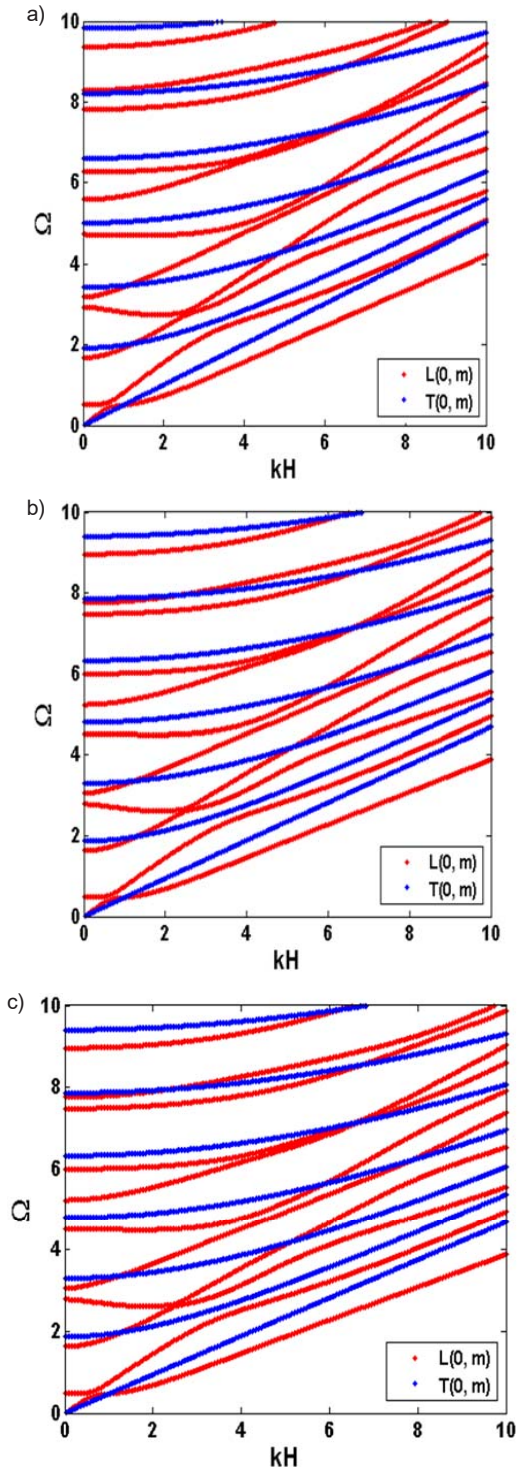

Fig. 5. Normalized frequency $\Omega = \omega H/(C_{44}/\rho)^{1/2}$ as a function of *kH* in the hollow cylinder for longitudinal and torsional modes (*n* = 0): (a) *S* = 0.1, (b) *S* = 1, (c) *S* = 4

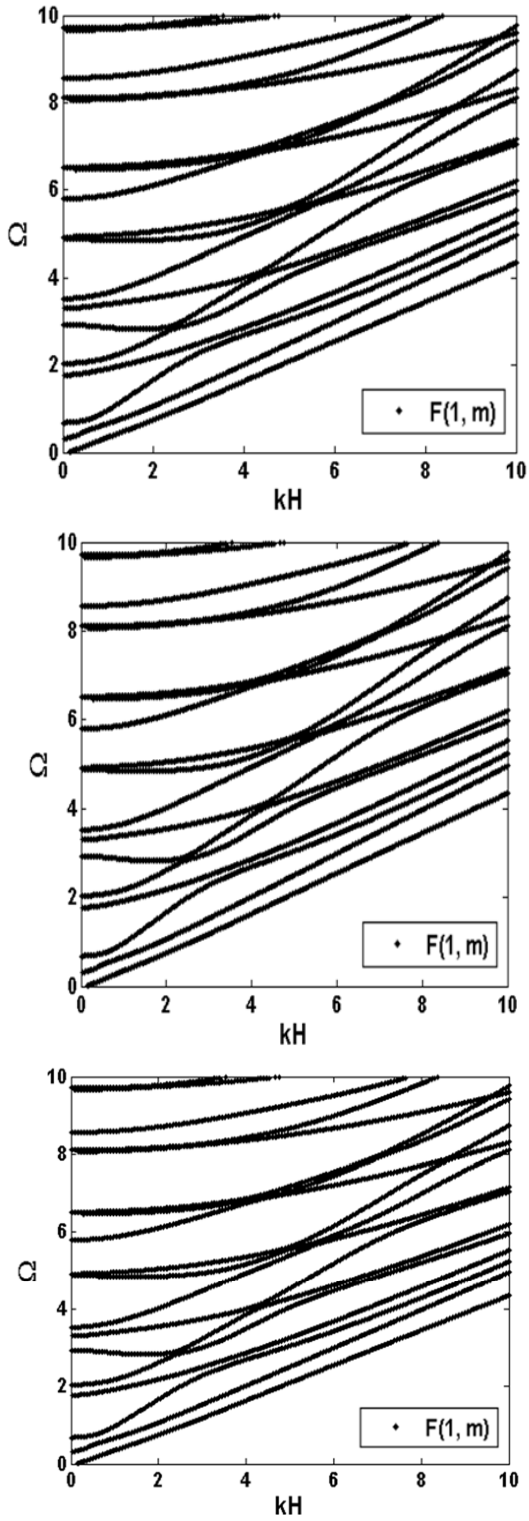

Fig. 6. Normalized frequency $\Omega = \omega H/(C_{44}/\rho)^{1/2}$ as a function of kH in the FGM hollow cylinder for symmetric modes (*n* = 1): (a) S = 0.1, (b) S = 1, (c) S = 4

off frequency. Fundamental modes L(0,1), T(0,1), and F(0,1) are the only modes that exist at extremely low frequencies. At higher frequencies, all the fundamental modes are transformed into Rayleigh surface waves and propagate at the Rayleigh speed $(V_R = 2940\ \mathrm{m/s})$.

It is clear that there is a relationship between the values of the graded index and phase velocity curves for L(0, 1) and T(0, 1) modes of the three-layered FGM cylinder. Furthermore, in both figures, the effects of the graded index on the cut-off frequencies differ in propagation modes that are symmetric and axisymmetric. The graded index has a considerable effect on the

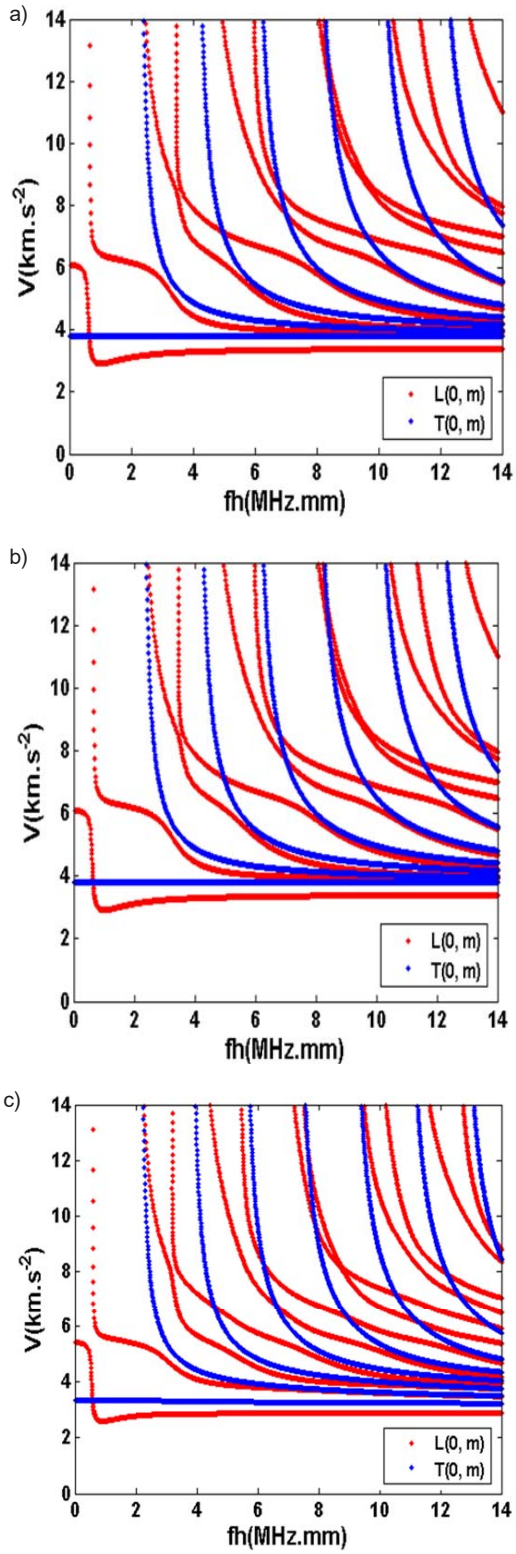

Fig. 7. Phase velocity dispersion curves as a function of the frequency-thickness product in the hollow FGM cylinder for longitudinal and torsional modes: (a) S = 0.1, (b) S = 1, (c) S = 4

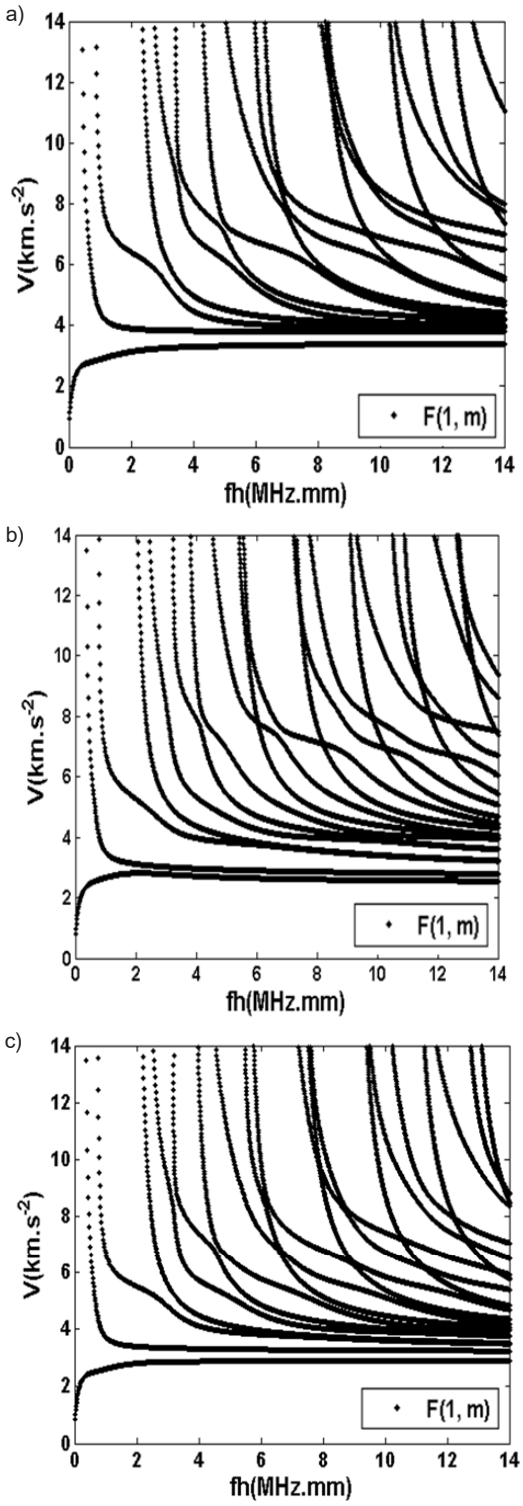

Fig. 8. Phase velocity dispersion curves as a function of the frequency-thickness product in the hollow FGM cylinder for flexural modes: (a) S = 0.1, (b) S = 1, (c) S = 4

phase velocity curves in longitudinal and torsional modes. Fig. 7a shows that the phase velocity of L(0,1) and T(0,1) modes is substantially higher than that in Figs. 7b and 7c for hollow FGM cylinders. These results demonstrate that the phase velocities of the same mode decrease as the exponents of the power law increase. This can be explained by the fact that small values of *s* correlate to the large volume fractions of stainless steel (Figure 2a V_{m1}), while the large values of *s*

correlate to the small volume fractions of silicon nitride (Figure 2b V_{m2}).

Mechanical displacements and stress distributions

In this section, the conundrum lays in determining the profiles of the mechanical displacements and normal stresses corresponding to different normalized frequencies, through the thickness of the cylinder. Therefore, we examined the normal stresses and mechanical displacement profiles for the axisymmetric (n = 0) and non-axisymmetric modes (n = 1) in the hollow inhomogeneous functionally graded cylinder. Figs. 9 and 10 show the mechanical displacement profiles for both axisymmetric (n = 0) and non-axisymmetric (n = 1) modes, respectively. In case of longitudinal modes, the circumferential component v always remains zero along the cylinder thickness, whereas the axial component dominates in the mechanical displacements. However, the axial and radial components are zero for torsional modes. In case of flexural modes, as opposed to compression and torsional modes, each component of the mechanical displacement is coupled with each and every other component.

Stress distributions and boundary conditions

Figs. 11 and 12 show the normal stress profiles of the hollow FGM cylinder for longitudinal modes (n = 0) and flexural modes (n = 1), respectively. As can be observed, in case of axisymmetric modes, the circumferential stresses $T_{r\varphi}$ are zero, while in case of flexural modes they are very low. In case of axisymmetric and flexural modes, it is evident that all normal stresses are zero on the inner and outer surfaces of the cylinder. This demonstrates the effectiveness of the mathematical approach employed to establish the boundary conditions. Although the elastic constants of two adjoining layers differ, it is widely known that at the interfaces, the normal stresses and displacements vary continuously from one surface to the next due to the advantages of monotonic fluctuation in the volume fraction of the component phases. All higher order modes propagate inside the cylinder, and the motion of the particles becomes more complicated. The latter is what explains why all the constraints are zero at the edges of the cylinder.

Method validation

In the course of the study, we investigated the dispersion curves of the guided waves propagating through the hollow inhomogeneous FGM cylinder of the (SS/SN/SS) configuration with various gradient shapes. For this purpose, a computer program using the Legendre polynomial approach based on the previous formulations was implemented

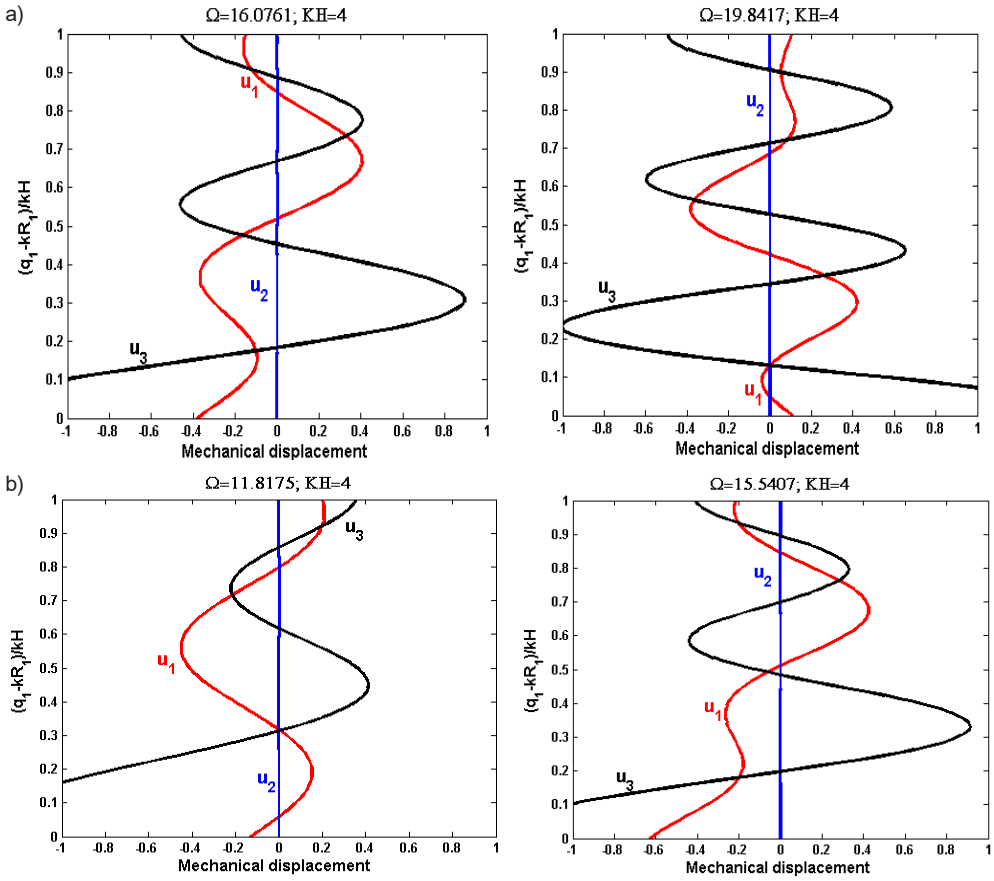

Fig. 9. Normalized mechanical displacement profiles of the hollow cylinder in case of longitudinal modes, n = 0, H/R = 4.00 for (SN/SS/SN): (a) S = 1, (b) S = 4

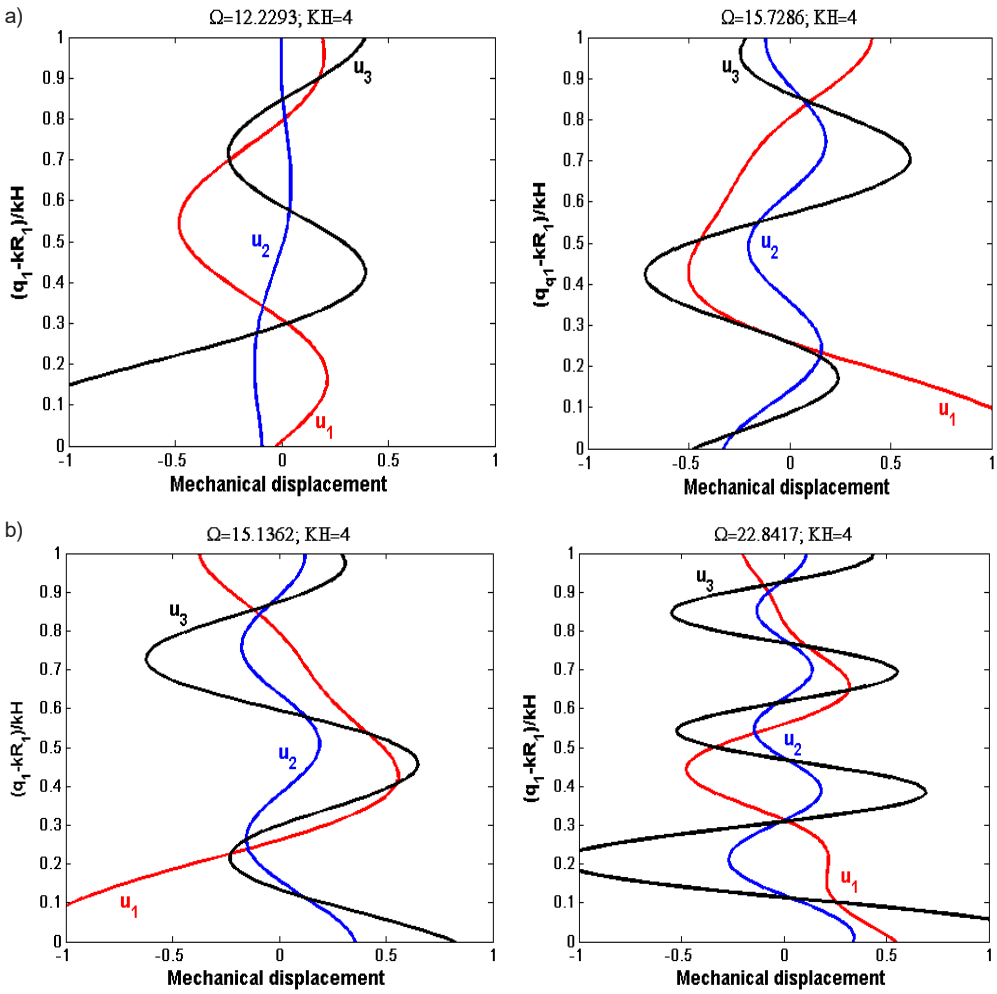

Fig. 10. Normalized mechanical displacement profiles of the hollow cylinder in case of flexural modes, n = 1, H/R = 4.00: (a) S = 1, (b) S = 4

in MATLAB software. The dispersion curves of normalized frequencies and phase velocity for three layers of FGM with a cylindrical shape are completely undetermined. As shown in Fig. 13, to compare our results with the available data (Gong et. al., 1999; Hedayatrasa et al., 2014), we calculate the normalized frequencies of the hollow FGM cylinder with two layers made of stainless steel and silicon nitride. Simulations are made considering the axisymmetric mode (n = 0) with three different gradient index S values for a specific limit when kR = 20kH with truncation M = 25. The comparison of our results with those reported in literature by Han et al. (2002) demonstrates that our methods has a high degree of precision and reliability in addition to the theoretical and programming equation accuracy.

It is clearly observed that the results of the numerical analytical method (reported by Han et al. (2002)) are compatible with the results obtained with the use of our method. This approach can predict the behavior of an infinite-length FGM cylinder with quite a high accuracy. The comparison of our findings with those found in literature demonstrates that our method has a high degree of accuracy and reliability.

Conclusion

The goal of the study was to develop a numerical approach to solve and compute the wave propagation problem in a continuous three-layered FGM cylinder, without discretizing the gradient structure. The polynomial approach considerably reduced the challenges experienced in this context and offered access to more rapid and precise numerical results. The propagation characteristics of the guided waves in three-layered FGM cylinders were determined. The obtained results showed that the variations of the material properties in the radial direction are significantly influenced by the graded index. The dispersion curves of the normalized frequencies and phase velocities are considerably impacted by the graded index due to the continuous variation of the volume fraction. The influence of the boundary conditions on the normal stresses across the radial direction of FG material was examined. Based on the simulations, it was found that the field profiles are strongly influenced by the

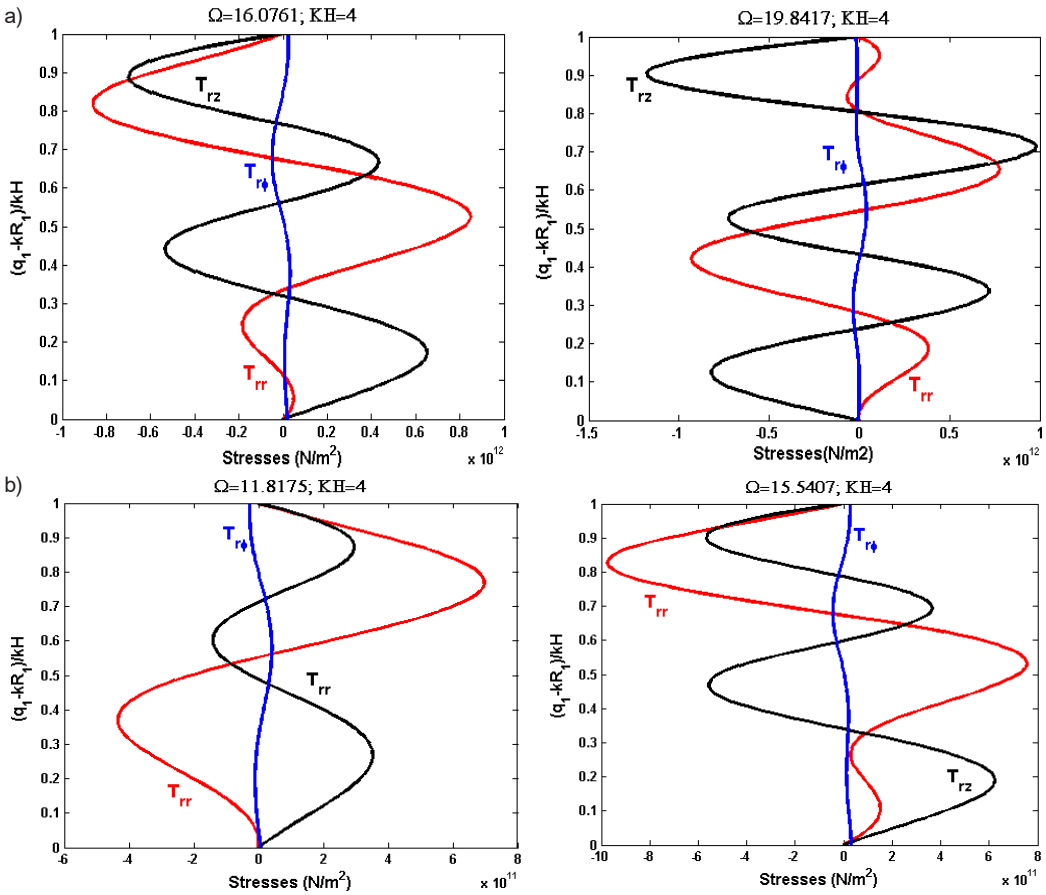

Fig. 11. Normal stress profiles for the first six modes in case of longitudinal modes (n = 0), H/R = 4.00 for (SN/SS/SN): (a) S = 1, (b) S = 4

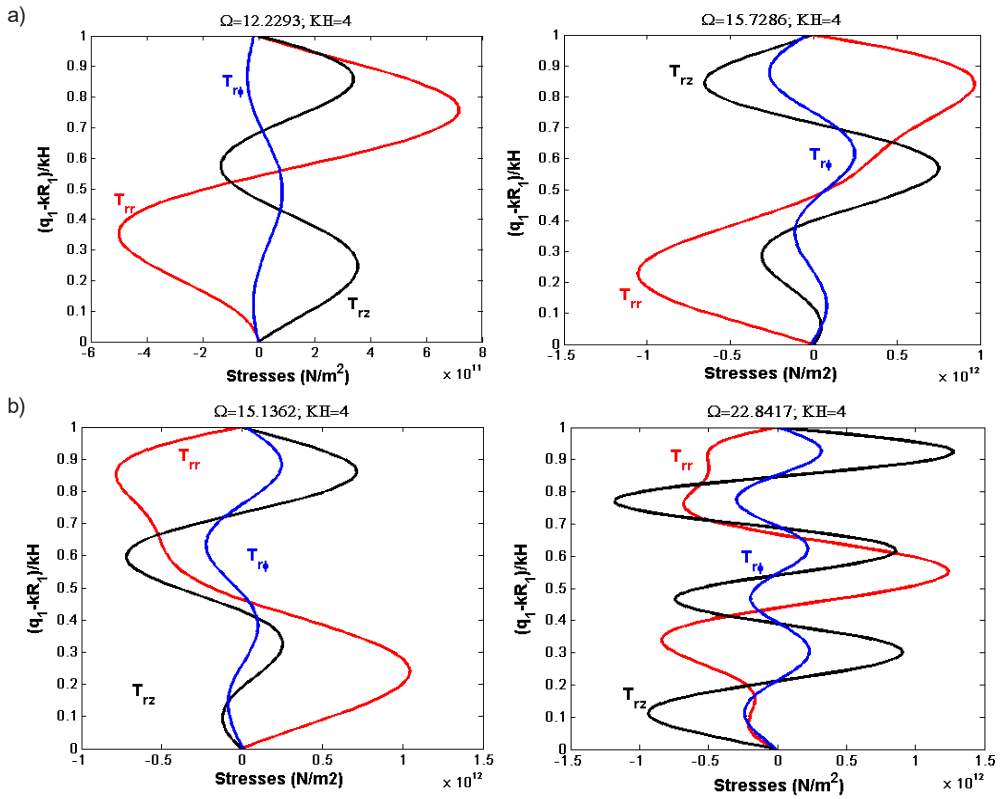

Fig. 12. Normal stress profiles in case of flexural modes (n = 0), H/R = 4.00: (a) S = 1, (b) S = 4

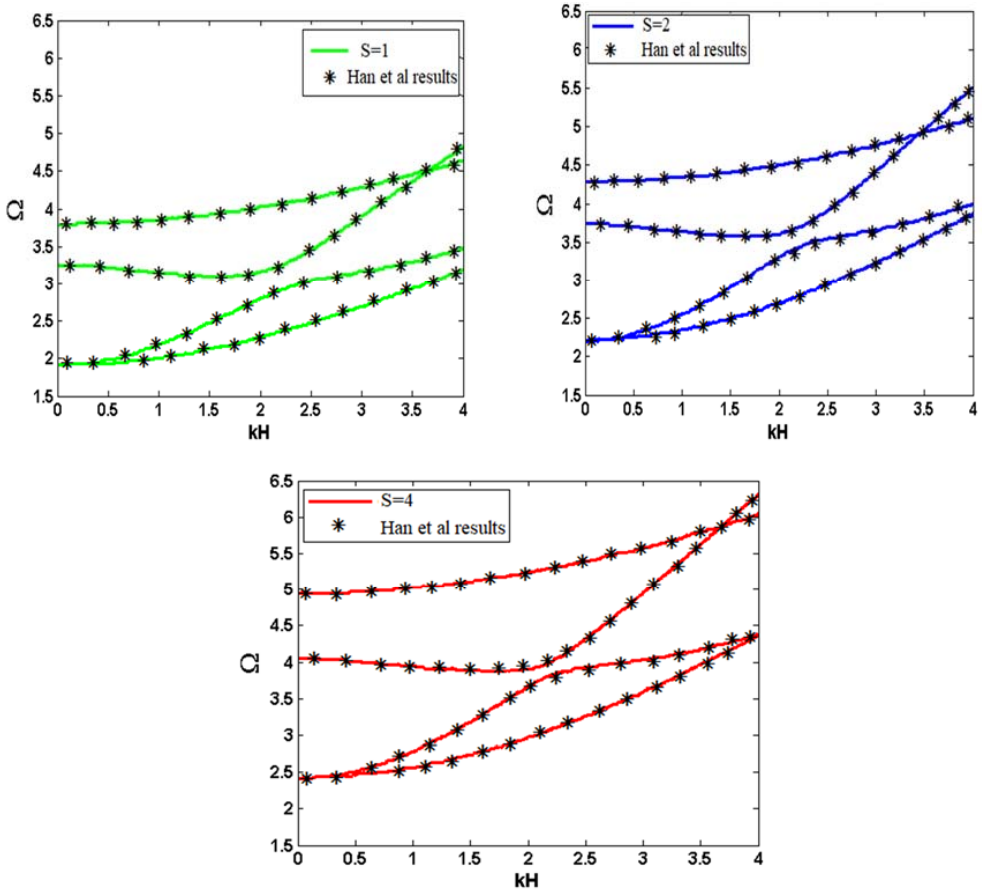

Fig. 13. Comparison for the normalized frequency using the results obtained by Han et al. (2022) and the results obtained by the polynomial method at $n = 0$ and $R = 20H$

electrical and mechanical boundary conditions. The comparisons with the results published in literature showed that the Legendre polynomial approach can model the propagation of acoustic waves in a three-dimensional FGM cylinder. The results reveal that the current approach is extremely accurate when compared to other available reference data. All acoustic eigenmodes, regardless of their kind, can be precisely identified due to the fast convergence of the presented method.

Appendix

The elements required to calculate the eigenvalues and eigenvectors:

$$ {}^{l}A_{11}^{m,j} = \frac{1}{(kH)^{l}} \left\{ \begin{bmatrix} C_{11}^{(l)\,l+2} I_{m,j}^{3} + (1+l) C_{11}^{(l)\,l+1} I_{m,j}^{2} + \\ +(lC_{12}^{(l)} - C_{22}^{(l)} - n^{2} C_{66}^{(l)})^{l} I_{m,j}^{1} - C_{55}^{(l)\,l+2} I_{m,j}^{1} \end{bmatrix} \pi(ka,kb) + \right. $$
$$ \left. + \left(C_{12}^{(l)\,l+1} K_{m,j}^{1} + C_{11}^{(l)\,l+2} K_{m,j}^{2} \right) \left(\delta(q_1 = ka) - \delta(q_1 = kb) \right) \right\}; $$

$$ {}^{l}A_{12}^{m,j} = \frac{1}{(kH)^{l}} \left\{ \begin{bmatrix} -in(C_{12}^{(l)} + C_{66}^{(l)})^{l+1} I_{m,j}^{2} + \\ +in(lC_{22}^{(l)} - C_{66}^{(l)} - C_{12}^{(l)})^{l} I_{m,j}^{1} \end{bmatrix} \times \pi(ka,kb) + inC_{12}^{(l)\,l+1} K_{m,j}^{1} \left(\delta(q_1 = ka) - \delta(q_1 = kb) \right) \right\}; $$

$$ {}^{l}A_{13}^{m,j} = \frac{1}{(kH)^{l}} \left\{ \begin{bmatrix} -i(C_{13}^{(l)} + C_{55}^{(l)})^{l+2} I_{m,j}^{2} - \\ -i((1+l)C_{13}^{(l)} - C_{23}^{(l)})^{l+1} I_{m,j}^{1} \end{bmatrix} \pi(ka,kb) - iC_{13}^{(l)\,l+2} K_{m,j}^{2} \left(\delta(q_1 = ka) - \delta(q_1 = kb) \right) \right\}; $$

$$ {}^{l}A_{21}^{m,j} = \frac{1}{(kH)^{l}} \left\{ \begin{bmatrix} in(C_{12}^{(l)} + C_{66}^{(l)})^{l+1} I_{m,j}^{2} + \\ +in(C_{22}^{(l)} + (1+l) C_{66}^{(l)})^{l} I_{m,j}^{1} \end{bmatrix} \times \pi(ka,kb) + C_{66}^{(l)\,l+1} K_{m,j}^{1} \left(\delta(q_1 = ka) - \delta(q_1 = kb) \right) \right\}; $$

$$ {}^{l}A_{22}^{m,j} = \frac{1}{(kH)^{l}} \left\{ \begin{bmatrix} -(n^{2} C_{22}^{(l)} + (1+l) C_{66}^{(l)})^{l} I_{m,j}^{1} + \\ C_{66}^{(l)\,l+2} I_{m,j}^{3} + (1+l) C_{66}^{(l)\,l+1} I_{m,j}^{2} - C_{44}^{(l)\,l+2} I_{m,j}^{1} \end{bmatrix} \pi(ka,kb) + \right. $$
$$ \left. + C_{66}^{(l)} \left({}^{l}K_{m,j}^{2} - {}^{l+1}K_{m,j}^{1} \right) \left(\delta(q_1 = ka) - \delta(q_1 = kb) \right) \right\}; $$

$$ {}^{l}A_{23}^{m,j} = \frac{1}{(kH)^{l}} n(C_{23}^{(l)} + C_{44}^{(l)})^{l+1} I_{m,j}^{1} \pi(ka,kb); $$

$$ {}^{l}A_{31}^{m,j} = \frac{1}{(kH)^{l}} \left\{ \begin{bmatrix} -i(C_{13}^{(l)} + C_{55}^{(l)})^{l+2} I_{m,j}^{2} - i(C_{23}^{(l)} + \\ +(1+l) C_{55}^{(l)})^{l+1} I_{m,j}^{1} \end{bmatrix} \pi(ka,kb) - i^{\,l+2} K_{m,j}^{1} \left(\delta(q_1 = ka) - \delta(q_1 = kb) \right) \right\}; $$

$$ {}^{l}A_{32}^{m,j} = \frac{1}{(kH)^{l}} n(C_{23}^{(l)} + C_{44}^{(l)})^{l+1} I_{m,j}^{1} \pi(ka,kb); $$

$$ {}^{l}A_{33}^{m,j} = \frac{1}{(kH)^{l}} \left\{ \begin{bmatrix} C_{55}^{(l)\,,l+2} I_{m,j}^{2} - n^{2} C_{44}^{(l)\,l} I_{m,j}^{1} - \\ -C_{33}^{(l)\,l+2} I_{m,j}^{1} + (1+l) C_{55}^{(l)\,l+1} I_{m,j}^{2} \end{bmatrix} \pi(ka,kb) + C_{55}^{(l)\,l+2} K_{m,j}^{2} \left(\delta(q_1 = ka) - \delta(q_1 = kb) \right) \right\}; $$

$$ {}^{l}M_{m}^{j} = -\frac{\rho^{(l)}}{(kH)^{l}} \pi(ka,kb), $$

where:

$$ {}^{l}I_{m,j}^{1} = \int_{kR_1}^{kR_2} Q_j^{*} q_1^{l} Q_m(q_1) dq_1 = \langle Q_j | q_1^{l} | Q_m \rangle; $$

$$ {}^{l}I_{m,j}^{2} = \int_{kR_1}^{kR_2} Q_j^{*} q_1^{l} \frac{\partial Q_m(q_1)}{\partial q_1} dq_1 = \langle Q_j | q_1^{l} \frac{\partial}{\partial q_1} | Q_m \rangle; $$

$$ {}^{l}I_{m,j}^{3} = \int_{kR_1}^{kR_2} Q_j^{*} q_1^{l} \frac{\partial^{2} Q_m(q_1)}{\partial q_1^{2}} dq_1 = \langle Q_j | q_1^{l} \frac{\partial^{2}}{\partial q_1^{2}} | Q_m \rangle; $$

$$ {}^{l}K_{m,j}^{1} = \int_{kR_1}^{kR_2} Q_j^{*} q_1^{l} \frac{\partial \pi(ka,kb)}{\partial q_1} Q_m(q_1) dq_1 = \langle Q_j | q_1^{l} \frac{\partial \pi(ka,kb)}{\partial q_1} | Q_m \rangle; $$

$$ {}^{l}K_{m,j}^{2} = \int_{kR_1}^{kR_2} Q_j^{*} q_1^{l} \frac{\partial Q_m(q_1)}{\partial q_1} \frac{\partial \pi(ka,kb)}{\partial q_1} dq_1 = \langle Q_j | q_1^{l} \frac{\partial \pi(ka,kb)}{\partial q_1} \frac{\partial}{\partial q_1} | Q_m \rangle. $$

References

Ashida, F., Morimoto, T., and Kuwahara, R. (2022). Adaptive control of an unsteady stress oscillation in a functionally graded multiferroic composite thin plate. *European Journal of Mechanics - A/Solids*, Vol. 95, 104643. DOI: 10.1016/j.euromechsol.2022.104643.

Bezzie, Y. M. and Woldemichael, D. E (2021). Effects of graded-index and Poisson's ratio on elastic-solutions of a pressurized functionally graded material thick-walled cylinder. *Forces in Mechanics*, Vol. 4, 100032. DOI: 10.1016/j.finmec.2021.100032.

Bian, P.-L., Qing, H., and Yu, T. (2022). A new finite element method framework for axially functionally-graded nanobeam with stress-driven two-phase nonlocal integral model. *Composite Structures*, Vol. 295, 115769. DOI: 10.1016/j.compstruct.2022.115769.

Elmaimouni, L., Lefebvre, J. E., Zhang, V., and Gryba, T. (2005). Guided waves in radially graded cylinders: a polynomial approach. *NDT & E International*, Vol. 38, Issue 5, pp. 344–353. DOI: 10.1016/j.ndteint.2004.10.004.

Ghatage, P. S., Kar, V. R., and Sudhagar, P. E. (2020). On the numerical modelling and analysis of multi-directional functionally graded composite structures: A review. *Composite Structures*, Vol. 236, 111837. DOI: 10.1016/j.compstruct.2019.111837.

Gong, S. W., Lam, K. Y., and Reddy, J. N. (1999). The elastic response of functionally graded cylindrical shells to low-velocity impact. *International Journal of Impact Engineering*, Vol. 22, Issue 4, pp. 397–417. DOI: 10.1016/S0734-743X(98)00058-X.

Han, X. and Liu, G. R. (2003). Elastic waves in a functionally graded piezoelectric cylinder. *Smart Materials and Structures*, Vol. 12, No. 6, pp. 962–971. DOI: 10.1088/0964-1726/12/6/014.

Han, X., Liu, G. R., Xi, Z. C., and Lam, K. Y (2002). Characteristics of waves in a functionally graded cylinder. *International Journal for Numerical Methods in Engineering*, Vol. 53, Issue 3, pp. 653–676. DOI: 10.1002/nme.305.

Hedayatrasa, S., Bui, T. Q, Zhang, C., and Lim, C. W (2014). Numerical modeling of wave propagation in functionally graded materials using time-domain spectral Chebyshev elements. *Journal of Computational Physics*, Vol. 258, pp. 381–404. DOI: 10.1016/j.jcp.2013.10.037.

Huang, S., Zhang, Y., Wei, Z., Wang, S., and Sun, H. (2020). *Theory and methodology of electromagnetic ultrasonic guided wave imaging*. Singapore: Springer, 289 p.

Lefebvre, J. E., Zhang, V., Gazalet, J., Gryba, T., and Sadaune, V. (2001). Acoustic wave propagation in continuous functionally graded plates: an extension of the Legendre polynomial approach. *IEEE Transactions on Ultrasonics, Ferroelectrics, and Frequency Control*, Vol. 48, Issue 5, pp. 1332–1340. DOI: 10.1109/58.949742.

Li, Z., Yu, J., Zhang, X., and Elmaimouni, L. (2022). Study on propagation characteristics of ultrasonic guided wave and detection of the defect in resin bolts. *Applied Acoustics*, Vol. 195, 108843. DOI: 10.1016/j.apacoust.2022.108843.

Liu, C., Yu, J., Zhang, B., Zhang, X., and Elmaimouni, L. (2021). Analysis of Lamb wave propagation in a functionally graded piezoelectric small-scale plate based on the modified couple stress theory. *Composite Structures*, Vol. 265, 113733. DOI: 10.1016/j.compstruct.2021.113733.

Naciri, I., Rguiti, A., Elmaimouni, L., Lefebvre, J.-E., Ratolojanahary, F. E, Yu, J. G., Belkassmi, Y., and El Moussati, A. (2019). Numerical modelling of vibration characteristics of a partially metallized micro electromechanical system resonator disc. *Acta Acustica united with Acustica*, Vol. 105, No. 6, pp. 1164–1172. DOI: 10.3813/AAA.919393.

Radman, A., Huang, X., and Xie, Y. M. (2013). Topology optimization of functionally graded cellular materials. Journal of Materials Science, Vol. 48, Issue 4, pp. 1503–1510. DOI: 10.1007/s10853-012-6905-1.

Velhinho A. and Rocha, L. A (2011). Longitudinal centrifugal casting of metal-matrix functionally graded composites: an assessment of modelling issues. *Journal of Materials Science*, Vol. 46, Issue 11, pp. 3753–3765. DOI: 10.1007/s10853-011-5289-y.

Wang, K., Cao, W., Xu, L., Yang, X., Su, Z., Zhang, X., and Chen, L. (2020). Diffuse ultrasonic wave-based structural health monitoring for railway turnouts. *Ultrasonics*, Vol. 101, 106031. DOI: 10.1016/j.ultras.2019.106031.

Wang, Q., Hu, S., Zhong, R., Bin, Q., and Shao, W. (2022). A local gradient smoothing method for solving the free vibration model of functionally graded coupled structures. *Engineering Analysis with Boundary Elements*, Vol. 140, pp. 243–261. DOI: 10.1016/j.enganabound.2022.04.015.

Wang, R. and Pan, E. (2011). Three-dimensional modeling of functionally graded multiferroic composites. *Mechanics of Advanced Materials and Structures*, Vol. 18, Issue 1, pp. 68–76. DOI: 10.1080/15376494.2010.519227.

Yang, Y. and Liu, Y. (2020). A new boundary element method for modeling wave propagation in functionally graded materials. *European Journal of Mechanics - A/Solids*, Vol. 80, 103897. DOI: 10.1016/j.euromechsol.2019.103897.

Yilmaz, C., Topal, S., Ali, H. Q., Tabrizi, I. E., Al-Nadhari, A., Suleman, A., and Yildiz, M. (2020). Non-destructive determination of the stiffness matrix of a laminated composite structure with lamb wave. *Composite Structures*, Vol. 237, 111956. DOI: 10.1016/j.compstruct.2020.111956.

Yu, J., Lefebvre, J. E., Guo, Y., & Elmaimouni, L. (2012). Wave propagation in the circumferential direction of general multilayered piezoelectric cylindrical plates. IEEE transactions on ultrasonics, ferroelectrics, and frequency control, 59(11), 2498-2508. DOI: 10.1109/TUFFC.2012.2482.

Yu, J., Wu, B., and He, C. (2010). Guided thermoelastic waves in functionally graded plates with two relaxation times. International Journal of Engineering Science, Vol. 48, Issue 12, pp. 1709–1720. DOI: 10.1016/j.ijengsci.2010.10.002.

Zhang, X., Li, Z., and Yu, J. (2018). The computation of complex dispersion and properties of evanescent Lamb wave in functionally graded piezoelectric-piezomagnetic plates. *Materials*, Vol. 11, Issue 7, 1186. DOI: 10.3390/ma11071186.

Zhang, B., Li, L. J., Yu, J. G., and Elmaimouni, L. (2022a). Generalized thermo-elastic waves propagating in bars with a rectangular cross-section. *Archive of Applied Mechanics*, Vol. 92, Issue 3, pp. 785–799. DOI: 10.1007/s00419-021-02072-3.

Zhang, B., Yu, J., Zhou, H., Zhang, X., and Elmaimouni, L. (2022b). Guided waves in a functionally graded 1-D hexagonal quasi-crystal plate with piezoelectric effect. *Journal of Intelligent Material Systems and Structures*, Vol. 33, Issue 13, pp. 1678–1696. DOI: 10.1177/1045389X211063952.

МОДЕЛИРОВАНИЕ СВОБОДНЫХ КОЛЕБАНИЙ В ПОЛОМ ФУНКЦИОНАЛЬНО-ГРАДИЕНТНОМ ЦИЛИНДРЕ С ПОМОЩЬЮ МЕТОДА ПОЛИНОМОВ ЛЕЖАНДРА

Рабаб Рагиб[1]*, Исмаил Насири[1], Хассна Хальфи[1], Лахусин эльмаймуни[1], Цзяньгун Юй[2], Абдельмаджид Биби[3], Мустафа Сахал[1]

[1]Лаборатория ПЕТИ-ЭРМАМ, Университет Ибн-Зор, полидисциплинарный факультет Варзазата, BP.638, 45000 Варзазат, Марокко
[2]Факультет механики и энергетики, Политехнический университет Хэнаня, Цзяоцзо 454003, Китай
[3]Университет Мохаммеда V в Рабате, Высшая школа технологий Сале, группа по материалам, энергии и акустике (MEAT), Марокко

*E-mail: rababraghib97@gmail.com

Аннотация
Введение: Строительная отрасль испытывает все большее давление в связи с тем, что требуется максимизировать эксплуатационные характеристики при одновременном снижении затрат и уменьшении воздействия на окружающую среду. Для решения этой проблемы предлагается новый тип материалов, а именно функционально-градиентные материалы (ФГМ). Преимущество этих материалов в том, что они способны выдерживать жесткие условия эксплуатации без потери своих свойств. **Цель исследования:** данная работа направлена на дальнейшее расширение представлений о типах распространения и характеристиках направленных волн в цилиндрах из ФГМ с бесконечной длиной. В ходе исследования мы проанализировали цилиндрическую оболочку, состоящую из трех кольцевых слоев, каждый из которых разделен градиентным слоем по толщине стенки. В статье предлагается инструмент моделирования, основанный на методе ортогональных полиномов Лежандра. **Методы:** применяемый метод приводит к проблеме собственных значений / собственных векторов. Граничные условия интегрируются в определяющие уравнения распространения направленных волн. Рассчитаны кривые дисперсии фазовой скорости и нормированной частоты. Кроме того, рассчитываются и рассматриваются распределения перемещений и профили поля напряжений для функционально-градиентного цилиндра с различными градиентными показателями в обоих типах (осесимметричном и симметричном). Результаты демонстрируют постоянные колебания в эффективном ФГМ. **Результаты:** было обнаружено, что кривые фазовой скорости одного и того же типа распространения уменьшаются с увеличением экспоненты степенного закона. Кроме того, граничные условия оказывают большее влияние на нормальные напряжения. Точность и эффективность усовершенствованного метода ортогональных полиномов демонстрируется на примере сравнения точного решения, полученного численно-аналитическим способом, и наших численных результатов.

Ключевые слова: направленные, метод полиномов Лежандра, функционально-градиентные материалы (ФГМ), кривые дисперсии.